EurJIC
European Journal of Inorganic Chemistry

A Journal of ChemPubSoc Europe

Accepted Article

Title: Next Generation of Guanidine Quinoline Copper Complexes for Highly Controlled ATRP: Influence of Backbone Substitution on Redox Chemistry and Solubility

Authors: Sonja Herres-Pawlis, Thomas Rösener, and Alexander Hoffmann

To be cited as: *Eur. J. Inorg. Chem.* 10.1002/ejic.201800511

Link to VoR: http://dx.doi.org/10.1002/ejic.201800511

WILEY-VCH

WILEY-VCH

FULL PAPER

Next Generation of Guanidine Quinoline Copper Complexes for Highly Controlled ATRP: Influence of Backbone Substitution on Redox Chemistry and Solubility

Thomas Rösener,[a] Alexander Hoffmann[a] and Sonja Herres-Pawlis*[a]

Abstract: Based on the guanidine quinoline (GUAqu) ligands 1,3-dimethyl-N-(quinolin-8-yl)-imidazolidin-2-imine (DMEGqu) and 1,1,3,3-tetramethyl-2-(quinolin-8-yl)-guanidine (TMGqu) the four ligands DMEG6etqu, TMG6etqu, DMEG6buqu and TMG6buqu were developed. These ligands feature an alkyl substitutent at C6 of the quinoline backbone. The synthetic strategy developed here allows inexpensive syntheses of any kind of C6 substituted GUAqu ligands. The alkylation on one hand increases the solubility of corresponding copper complexes in apolar ATRP monomers like styrene. On the other hand it has a significant electronic influence and thus an effect on the donor properties of the new ligands. Seven Cu^{I} and Cu^{II} complexes of DMEG6etqu and TMG6etqu have been crystallised and were studied with regards to their structural and electrochemical properties. Cu^{I} and Cu^{II} complexes of DMEG6buqu and TMG6buqu turned out to be perfectly soluble in pure styrene even at room temperature which makes them excellent catalysts in ATRP of apolar monomers. The key characteristics of the ATRP equilibrium K_{ATRP} and k_{act} were determined for the new complexes. In addition we used our recently developed DFT methodology, NBO analysis and isodesmic reactions to predict the influence of the introduced alkyl substituents. It turned out, that high conformational freedom in the complex structures leads to a significant uncertainty in prediction of the thermodynamic properties.

Introduction

Atom transfer radical polymerisation (ATRP) has become one of the most versatile reversible-deactivation radical polymerisation (RDRP) methods since its invention in 1995.[1] In ATRP transition metal complexes mediate an equilibrium between dormant and active radical chains (Scheme 1, bottom). The transition metal complex reversibly caps active radical chains with a halogen atom (usually Br· or Cl·). Due to this equilibrium few active radical species coexist and thus chain termination reactions can be effectively suppressed. RDRP techniques based on ATRP allow the application of air stable catalyst precursors, the drastic reduction of transition metal concentration and an even higher controllability.[2] Amongst other factors the polymerisation rate in ATRP highly depends on the nature of the catalyst, which itself depends mainly on the ligand environment. Thus, in copper ATRP a large variety of different N-donor ligands has been evaluated and structure reactivity relationships were derived. The activity of a copper complex in ATRP is influenced by the denticity of the ligand, the nature of the N-donor and its electron donating ability.[3] The analysis of different 4,4'-substituted 2,2'-bipyridine (top left of Scheme 1) ligands furthermore exhibited the effect of ligand substitution on the catalyst activity.[4] The most active ATRP catalyst so far features the tetrapodal ligand $TMPA^{NMe2}$ (top middle of Scheme 1, R = NMe_2). Copper complexes of $TPMA^{NMe2}$ show K_{ATRP} values of about 1.[5]

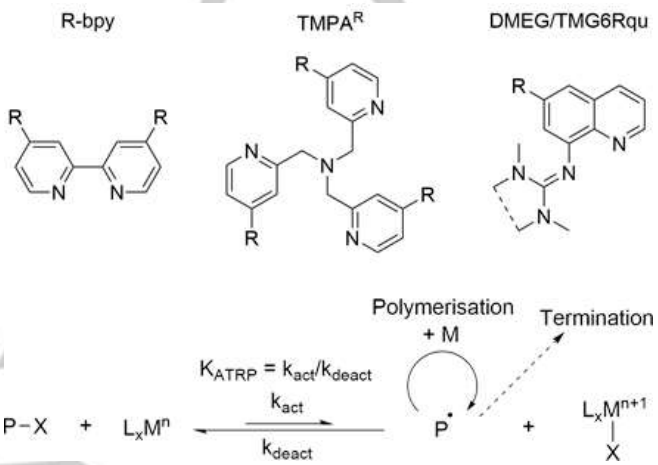

Scheme 1. The ATRP equilibrium and substitution at known ATRP ligands[3,4]

In the past, we focused on the implementation of a new and promising ligand class in ATRP, the guanidine ligands.[6–11] Since guanidines represent a class of strong and neutral N-donors, they have great potential in ATRP. Guanidine ligands already found broad application in the field of homogenous catalysis. Recent publications describe the application in the ring opening polymerisation (ROP) of lactide[12] or oxygen activation.[13] Nevertheless only few examples of guanidine complexes in ATRP are known.[6–11,14]

Recently, we showed that copper complexes of the bidentate guanidine quinoline (GUAqu) ligands DMEGqu and TMGqu (top right of Scheme 1, R = H) possess redox potentials that are comparable to the tridentate ligand PMDETA. ATRP reactions could be successfully conducted.[6] These ligands also recently attracted attention in the fields of copper photochemistry[15] and as entatic state models for electron transfer proteins.[16] A targeted improvement of GUAqu ligands thus is the next logical step.

[a] T. Rösener, Dr. A. Hoffmann, Prof. Dr. S. Herres-Pawlis
Institut für Anorganische Chemie
RWTH Aachen University
Landoltweg 1, 52074 Aachen (Germany)
sonja.herres-pawlis@ac.rwth-aachen.de
http://www.bioac.ac.rwth-aachen.de/

Supporting information for this article is given via a link at the end of the document.

A major drawback of GUAqu copper halogenido complexes with regard to ATRP was their bad solubility in apolar monomers like styrene. So we target herein the improvement of the GUAqu ligands for a better solubility of corresponding complexes. We present a new synthetic pathway for the synthesis of C6-substituted GUAqu ligands and will herein focus on the synthesis of the alkyl substituted ligands DMEG6etqu, TMG6etqu, DMEG6buqu and TMG6buqu. The corresponding copper halide complexes were investigated towards their molecular structures, redox potential and properties in ATRP.

Matyjasewski *et al.* established a linear correlation of the redox potential and lg(K_{ATRP}). By solely knowing the redox potential of the activator/deactivator couple, the value for K_{ATRP} and consequently the activity of the catalyst can be estimated.[17] The evaluation of new ATRP catalysts with respect to their activity thus became much easier. In addition, efforts have been made to calculate $E_{1/2}$ of certain compounds via DFT. Unfortunately, the uncertainty of these methods is too high when it comes down to small differences.[18] As we showed earlier, systematic errors in calculation can be overcome with the concept of the isodesmic reaction and, as long as there is structural data available, correct predictions can be made.[6,19]

Since the alkyl substituent has an influence on the donor properties of the ligands, we tried to predict the thermodynamic properties of the new catalyst with our computational method. We investigated whether the influence of the alkyl substituents can be predicted correctly even when there is no structural data available and whether DFT might be a tool for the targeted syntheses of new ligands in ATRP.

Results and Discussion

Synthesis of the ligands

Development of Alkylated Guanidine Quinoline Ligands

In order to improve the solubility of copper guanidine quinoline complexes in apolar monomers, the quinoline backbone of the ligands was alkylated. Beside its effect on the solubility, such an alkyl substituent has a positive electronic effect on the donor properties of the ligands. With the help of DFT and subsequent NBO calculations we estimated, at which position the alkyl substituent has its maximal influence. All possible substitution positions are depicted in Scheme 2.

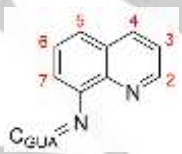

Scheme 2. Possible substitution positions (in red) on GUAqu.

Starting geometries of substituted DMEG***n***alkqu and TMG***n***alkqu (where ***n*** is the position of substitution) ligands and the unsubstituted Ligand TMGqu were generated from the molecular structure of DMEGqu. To evaluate the electronic influence of an ethyl-substituent at the different positions, the starting geometries were first optimised using our methodology in Ref.[6]. This DFT methodology includes the basis set def2-TZVP,[20] the hybrid functional TPSSh[21] and empirical dispersion with Becke-Johnson damping GD3BJ.[22–24] Since acetonitrile was used as solvent in most of our reactions, all calculations were performed with a SMD model for acetonitrile.[25] The structural optimisations were followed by NBO calculations. NBO charges give hints to the donor properties of the ligands.[6] Considering that the ethyl-substituent has an influence on both the guanidine and quinoline donor, the NBO charges of these donors were added up. A more negative sum of charges suggests overall better donor properties of the ligand. The results for differently substituted DMEG***n***etqu and TMG***n***etqu are summarised in Table 1.

Table 1. NBO charges of N_{GUA} and N_{qu} in different substituted GUA***n***etqu-ligands and the unsubstituted ligands DMEGqu and TMGqu. Highest absolute sum of charges highlighted (TPSSh/def2-TZVP; GD3BJ; SMD: MeCN).

NBO charges [e⁻]

	DMEG*n*etqu			**TMG*n*etqu**		
Position	N_{GUA}	N_{qu}	Sum	N_{GUA}	N_{qu}	Sum
unsub.	-0.595	-0.441	-1.036	-0.595	-0.431	-1.026
C2	-0.597	-0.455	-1.052	-0.593	-0.444	-1.036
C3	-0.593	-0.434	-1.027	-0.593	-0.420	-1.013
C4	-0.593	-0.447	-1.041	-0.594	-0.439	-1.033
C5	-0.596	-0.442	-1.038	-0.596	-0.434	-1.030
C6	-0.599	-0.441	-1.040	-0.597	-0.434	-1.031
C7	-0.594	-0.444	-1.038	-0.592	-0.438	-1.030

An ethyl substituent in position C3 seems to decrease the overall charge in comparison with the unsubstituted ligand and was therefore ruled out as possible substitution position. Substitution in positions C2, C4, and C6 on the other hand has the largest influence on the donor atoms in increasing the charge. Substitution on C2 might have a significant steric effect on the coordination chemistry and was thus also ruled out. Substitution at position C6 is synthetically much easier in comparison with the C4 and thus became our position of choice to modify the original ligand.

Synthetic Strategy

The synthetic strategy to obtain the target ligands requires no late transition metal cross-coupling reactions and hence, is easy scalable and rather inexpensive. The fundamental steps for the synthesis of the ligand precursor $NH_2$6alkqu are shown in Scheme 3. Different alkylated guanidine quinoline ligands can be synthesised starting from commercially available 4-alkylated anilines. Thus, with our synthetic approach and appropriate anilines at hands, a whole library of differently C6 substituted guanidine quinoline ligands can be synthesised.

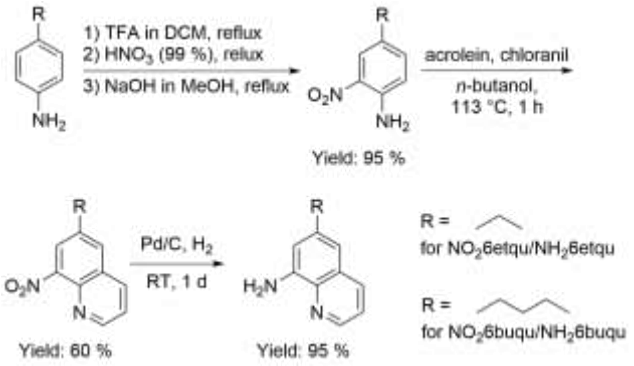

Scheme 3. Synthetic access to $NH_2$6alkqu. R = different alkyl-substituents.

Herein, the ligand precursors $NH_2$6etqu (with an ethyl substituent at 6-position of qu) and $NH_2$6buqu (with a *n*-butyl substituent at 6-position of qu) were synthesised as starting materials for the four new ligands.

For $NH_2$6etqu, first nitration was accomplished following a slightly modified literature procedure by Buszek *et al*..[26] Instead of acetamide, trifluoroacetamide was used as protecting group for the amine function. The modified protection step runs at lower temperatures and thus, hazardous dichloroethane could be replaced by dichloromethane as solvent. In the next step, $NO_2$6etqu was synthesised according to a protocol by Wielgosz-Collin *et al*.[27] In this modified Skraup synthesis, the nitrated aniline was transformed into the corresponding quinoline. Afterwards, the nitro-quinoline was reduced to $NH_2$6etqu. $NH_2$6buqu was made analogously from 4-*n*-butylaniline. Experimental details for all steps are summarised in the SI.

Synthesis of the ligands

Starting from the ligand precursors $NH_2$6etqu and $NH_2$6buqu the four new ligands DMEG6etqu (**L1**), TMG6etqu (**L2**), DMEG6buqu (**L3**) and TMG6buqu (**L4**) were synthesised according to a general procedure (Scheme 4).[28,29]

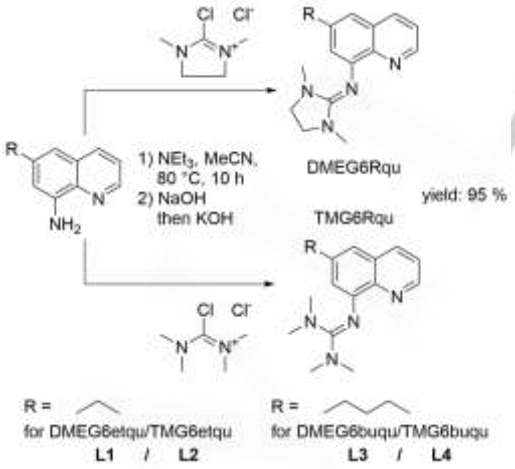

Scheme 4. Synthesis of differently substituted DMEG6alkqu and TMG6alkqu ligands.

The raw ligands appear as yellow brownish solids (**L1**) or highly viscous liquids (**L2-L4**), which had to be purified for their application in *in situ* K_{ATRP} or k_{act} measurements and polymerisation kinetics. **L1** was purified by sublimation, whereas **L2-L4** were purified by column chromatography. The pure ligands appear as yellow crystalline solids (**L1, L3**) or highly viscous liquids (**L2, L4**). Experimental details for synthesis and purification are summarised in the SI. Crystals of **L1** and **L3** were suitable for X-ray crystallography. The molecular structures are depicted in Figure S1, key structural parameters are summarised in Table S1 in the SI.

Synthesis and structural characterisation of the complexes

The reaction of DMEG6etqu and TMG6etqu with various anhydrous Cu^{I} and Cu^{II} halide salts resulted in crystals suitable for X-ray crystallography, whereas complexes of DMEG6buqu and TMG6buqu could not be crystallised. Thus with $Cu^{I}Br$, $Cu^{I}Cl$, $Cu^{II}Br_2$ and $Cu^{II}Cl_2$ eight complexes, namely $[Cu(DMEG6etqu)_2]Br$, $[Cu(DMEG6etqu)_2]Cl$, $[Cu(TMG6etqu)_2]Br$, $[Cu(TMG6etqu)_2]Cl$, $[Cu(DMEG6etqu)_2Br]Br$, $[Cu(DMEG6etqu)_2Cl]Cl$ $[Cu(TMG6etqu)_2Br]Br$, $[Cu(TMG6etqu)_2Cl]Cl$ could be structurally characterised. The crystallographic data of $[Cu(TMG6etqu)_2Br]Br$ was insufficient for publication and therefore is not discussed herein. Molecular structures of the chlorido complexes are exemplarily shown in Figure 1. Molecular structures of the bromido complexes are depicted in figure S2.

Table 2 summarises key bond lengths and angles of the copper GUA6etqu complexes. All Cu^{I} complexes comprise a cationic unit containing a copper centre coordinated by two GUA6etqu ligands in a distorted tetrahedron. A closer look on the geometrical properties in the $[Cu(DMEG6etqu)_2]Br$ and $[Cu(DMEG6etqu)_2]Cl$ complexes reveals significant but small differences between both structures although they only differ in their non-coordinating counter-ion. We ascribe this to packing effects in solid state, and this effect was also found in crystal structures of $[Cu(TMGqu)_2]^+$ with the counterions Cl^-, Br^- and ClO_4^-.[6,30] The differences in key bond lengths in the complexes $[Cu(TMG6etqu)_2]Br$ and $[Cu(TMG6etqu)_2]Cl$ on the other hand are insignificant, whereas the angles around the central metal also vary notably. N_{GUA}-Cu bond lengths in $[Cu(DMEG6etqu)_2]Br$ are significantly prolonged in comparison with $[Cu(TMG6etqu)_2]Br$. As noticed earlier the TMG moiety is the stronger donor compared to the DMEG moiety.[6] This is expressed in shorter N_{GUA}-Cu bond lengths in Cu^{I} complexes featuring TMG6etqu. In Cu^{II} complexes the metal centre is supplemented by a coordinating halide anion. Comparing $[Cu(DMEG6etqu)_2Cl]Cl$ and $[Cu(TMG6etqu)_2Cl]Cl$ it can be seen that the Cu-Cl bond length in the complex featuring TMG6etqu is significantly elongated. In comparison with the unsubstituted ligands one can see, that the introduction of an ethyl substituent in C6 position of the ligands leads to a shortening of the Cu-X bond in the case of DMEGqu and to an elongation of the same bond in the case of TMGqu.[6] To prove that complexes of the GUA6buqu ligands also form bischelate

Table 2. Key bond lengths and angles of the Cu^{I} complexes $[Cu(L)_2]X$ and the Cu^{II} complexes $[Cu(L)_2X]X$. L = DMEG6etqu or TMG6etqu and X = Cl or Br.

Bond lengths[Å]							
	Cu^{I}				**Cu^{II}**		
Ligand/ Cu-salt	DMEG6etqu/ CuBr	DMEG6etqu/ CuCl	TMG6etqu/ CuBr	TMG6etqu/ CuCl	DMEG6etqu / $CuBr_2$	DMEG6etqu/ $CuCl_2$	TMG6etqu/ $CuCl_2$
Cu-X (Cl/Br)	-	-	-	-	2.493(1)	2.319(1)	2.428(7)
Cu-N_{GUA} (1)	2.083(3)	2.154(3)	2.059(4)	2.067(6)	2.043(4)	2.022(3)	2.074(2)
Cu-N_{GUA} (2)	2.139(3)	2.154(3)	2.081(4)	2.088(6)	2.152(3)	2.211(3)	2.101(2)
Cu-N_{qu} (1)	1.985(3)	1.969(3)	2.002(4)	1.980(6)	1.989(4)	1.983(3)	1.982(2)
Cu-N_{qu} (2)	1.970(3)	1.969(3)	2.009(4)	1.963(6)	1.985(3)	1.999(3)	1.982(2)
Bond angles [°]							
N_{qu} (1)-Cu-N_{qu} (2)	145.2(2)	149.0(2)	146.2(2)	142.1(3)	178.2(2)	174.8(2)	178.3(1)
N_{GUA} (1)-Cu-X	-	-	-	-	137.7(1)	149.7(1)	125.9(2)
N_{GUA} (1)-Cu-N_{GUA} (2)	126.2(2)	131.5(2)	128.9(2)	116.2(2)	115.2(2)	110.1(1)	126.7(1)
Structure factors	**τ_4[a]**				**τ_5[b]**		
τ	0.63	0.56	0.60	0.72	0.68	0.42	0.87
ρ[c]	0.97	0.97	0.98	0.96	0.99	0.99	1.00

[a] $\tau_4 = \frac{360°-(\alpha+\beta)}{141}$. A τ_4 value of 1 is found in ideal tetrahedral complexes were a τ_4 value of 0 is found in ideal square planar complexes.[14] [b] $\tau_5 = \frac{(\alpha-\beta)}{60}$. A τ_5 value of 1 is found in ideal trigonal bipyramidal complexes were a τ_5 value of 0 is found in ideal square-based pyramidal complexes.[15] [c] $\rho = \frac{2a}{(b+c)}$ with a = d(C_{GUA}- N_{GUA}) and b and c = d(C_{GUA}- N_{amine}).[16] Average ρ-value of both guanidine moieties.

complexes in solution, a NMR experiment was carried out. The exemplary complex $[Cu(TMG6buqu)_2]Br$ was formed *in situ* in deuterated acetonitrile. Ligand and copper salt were used in a ratio of 2:1. Only one set of NMR signals could be detected in both ^{1}H- and ^{13}C-NMR spectra. This is an evidence that the bischelate complex is formed exclusively. Otherwise a second or even more sets of NMR signals should be found. The NMR spectra are depicted in Figures S36 and S37.

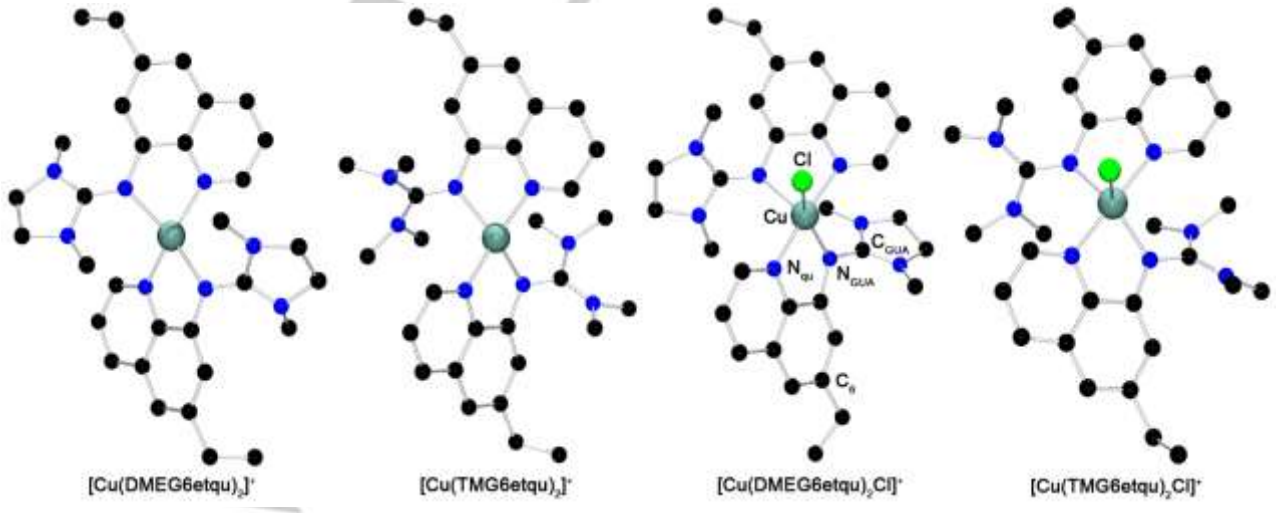

Figure 1. Molecular structures of the complex cations of the chlorido complexes. Key atoms are exemplarily marked in one complex. H atoms are omitted for clarity.

Electrochemistry

Since electrochemical properties provide information about the activity of copper complexes in ATRP, we performed cyclovoltammetric measurements (CV) to determine the redox potentials of our new catalysts. The measurements were done in acetonitrile starting from crystalline bischelate Cu^{II} complexes (GUA6etqu complexes) or bischelate Cu^{II} complexes generated *in situ* (GUA6buqu complexes). All measurements were carried out at room temperature at different sweep rates to proof reversible behavior of the redox process. $E_{1/2}$ was determined against the Fc/Fc^+ couple. Figure 2 shows cyclic voltammograms of the $[Cu^{I}(DMEG6etqu)_2Br]/[Cu^{II}(DMEG6etqu)_2Br]^+$ couple at different sweep rates. For better comparability with literature data the potentials were recalculated against SCE.[31]

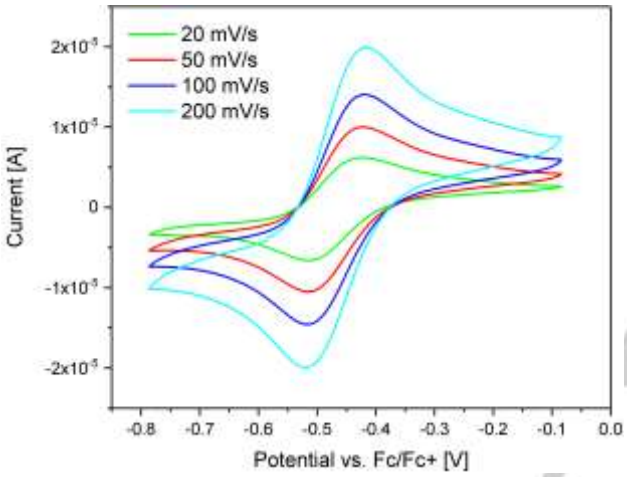

Figure 2. Cyclic voltammograms of the $[Cu^{I}(DMEG6etqu)_2Br]/[Cu^{II}(DMEG6etqu)_2Br]^+$ couple at different sweep rates starting from $[Cu(DMEG6etqu)_2Br]Br$.

Cyclovoltammetric measurements were performed starting from both Cu^{I} and Cu^{II} complexes of the ligands **L1 – L4**. Values for $E_{1/2}$ are listed in Tables S2 and S3. Starting from Cu^{I} or Cu^{II} complexes has only a negligible effect on the determined redox potentials. In relevant literature mostly redox potentials measured starting from Cu^{II} complexes are discussed, therefore in the following redox potentials measured this way are used for discussion. To illustrate the difference in redox potentials between all complexes, the half-wave potentials are depicted in Figure 3.

With introduction of electron donating alkyl substituents at C6 of the quinoline backbone we expected lower redox potentials for all new complexes, as better donating ligands stabilise the Cu^{II} complexes. In case of $[Cu(DMEG6buqu)_2Br]Br$ and $[Cu(DMEG6etqu)_2Br]Br$ almost no change in the redox potential could be observed which might be related to the weaker donor capability of the DMEG unit.[6] $CuBr_2$ complexes of TMG6alkqu ligands in contrast show redox potentials reduced by about 20 mV. $CuCl_2$ complexes of all GUA6alkqu ligands exhibit more negative redox potentials. The reduction of the redox potential is more pronounced in $CuCl_2$ complexes. While unsubstituted DMEGqu complexes are more reducing than analogous TMGqu complexes, this ratio is inverted in alkylated ligands. The influence of the alkyl substituent seems to be more pronounced in ligands including the TMG moiety.

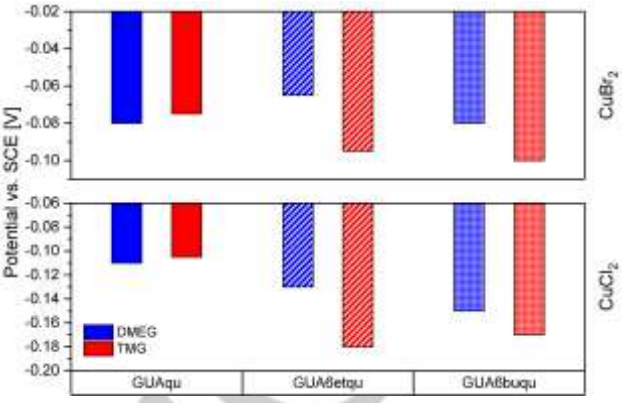

Figure 3. Redox potentials of various $[Cu^{I}L_2Br]/[Cu^{II}L_2Br]^+$ couples with L = GUAqu, GUA6etqu or GUA6buqu.

Based on the CV data we expected TMG6alkqu complexes with CuBr to be more active in ATRP in comparison with their unsubstituted counterpart $[Cu(TMGqu)_2Br]Br$. The activities of DMEG6alkqu complexes with CuBr should resemble the activity of $[Cu(DMEGqu)_2]Br$. For all further ATRP studies, we focused on the bromido complexes due to better comparability to other ATRP studies.[17,32]

Atom Transfer Radical Polymerisation

Determination of K_{ATRP}

K_{ATRP} is the central equilibrium constant of the ATRP equilibrium and represents the ratio of the rate constants of activation k_{act} and deactivation k_{deact}. Polymerisation velocity and control highly depend on K_{ATRP}.

Here, K_{ATRP} was determined by reacting CuBr complexes of the different GUA6alkqu ligands with the ATRP initiator ethyl α-bromoisobutyrate (EBrib) and following the evolution of the Cu^{II} species via UV/Vis spectroscopy. K_{ATRP} measurements for the previously reported systems featuring the ligands DMEGqu und TMGqu were repeated with the improved method to guarantee consistent conditions for all measurements.[6] Details about the procedure are summarised in the experimental section. For the UV/Vis spectroscopic determination of K_{ATRP} we followed the characteristic d-d transition band of the Cu^{II} complexes around 900-950 nm. Since the extinction coefficient ε of this UV/Vis absorption is essential for the determination of K_{ATRP} by the methods of Fisher and Fukuda and the method of Matyjaszewski, ε had to be determined precisely. Values for ε (Table S3) were determined from crystalline Cu^{II} complexes if possible. In the case of $[Cu(DMEG6buqu)_2Br]Br$ and $[Cu(TMG6buqu)_2Br]Br$ the complexes were generated *in situ*.

K_{ATRP} values were examined for all CuBr complexes of the new GUA6alkqu ligands at 22 °C in acetonitrile with EBrib as initiator. The measurements were repeated at least two times and the K_{ATPR} values arithmetically averaged.

Sample Matyjaszewski plots for all complexes are shown in Figures S3-S8. K_{ATRP} was calculated by the method developed by Matyjaszewski.[33] Values are summarised in Table 3.

Table 3. K_{ATRP} values for $[Cu(L)_2]Br$. L = GUAqu, GUA6etqu, GUA6buqu.

$[Cu(L)_2]Br$; L =	K_{ATRP} (Matyjaszewski)
DMEGqu	$9.0\pm0.7\times10^{-8}$
TMGqu	$8.6\pm0.5\times10^{-8}$
DMEG6etqu	$7.9\pm0.5\times10^{-8}$
TMG6etqu	$1.6\pm0.2\times10^{-7}$
DMEG6buqu	$7.8\pm0.7\times10^{-8}$
TMG6buqu	$1.34\pm0.04\times10^{-7}$

In Figure 4 the logarithmic values of K_{ATRP} (calculated by the method of Matyjaszewski) are plotted against $E_{1/2}$ determined via CV. All values roughly follow the correlation published by Matyjaszewski *et al*.[32]

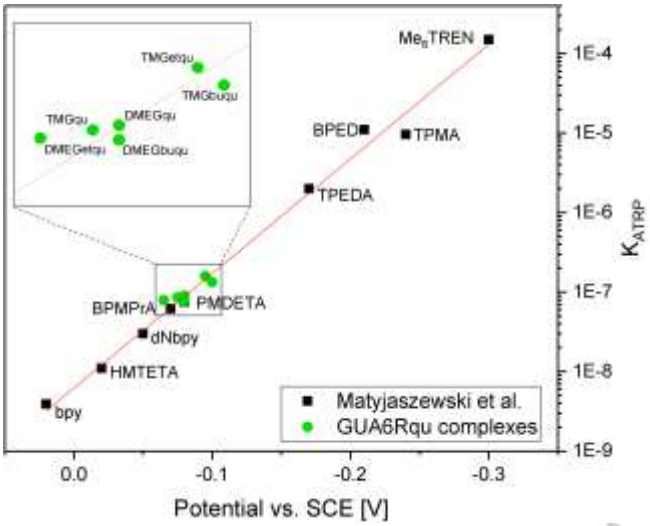

Figure 4. Correlation of $[Cu^{I}L_2Br]/[Cu^{II}L_2Br]^+$ redox potentials with K_{ATRP} values (measured with EBrib at 22 °C in MeCN). Black squares: Values published by Matyjaszewski *et al.*.[32] Green circles: Values for GUA6Rqu complexes.

Complexes of the bidentate GUAqu ligands exhibit redox potentials and values for K_{ATRP} comparable to complexes of the tridentate ligand PMDETA. Complexes of the substituted ligands TMG6etqu and TMG6buqu reveal the highest values for K_{ATRP} in comparison with all systems analysed herein. The ethyl/butyl substituent leads to an increase of electron density at the N-donor atoms and consequently stabilise Cu^{II} better than the original TMGqu ligand. On the other hand, ethyl/butyl substitution at C6 of DMEGqu leads to no significant change of K_{ATRP}. Based on these results we expected TMG6buqu complexes to be more active in ATRP.

Determination of k_{act} and k_{deact}:

Besides K_{ATRP}, the rate constant of deactivation k_{deact} is another important constant for the characterisation of newly developed ATRP catalysts. For the establishment of functional ARGET ATRP reactions the knowledge of k_{deact} is indispensable. Unfortunately, the direct measurement of k_{deact} is rather complicated.[34] The rate constant of activation k_{act} on the other hand can be easily determined via time-dependent UV/Vis spectroscopy. For the measurement a protocol published by Matyjaszewski *et al.* was applied.[35] The respective activator complex is reacted with a tenfold excess of the initiator (EBrib) to guarantee pseudo-first-order conditions. Addition of a trapping agent (2,2,6,6,-tetramethylpiperidinyl-1-oxyl, TEMPO) makes the activation step irreversible. Here, a tenfold excess with respect to the Cu^{I} complex was used as well. The formation of the Cu^{II} (deactivator) species was followed by UV/Vis spectroscopy. The same d-d absorption band (Table S4) as within the K_{ATRP} determination was used. The time-dependent evolution of the Cu^{II} complex can be fitted by the monoexponential equation $A = A_0(1 - e^{-k_{obs}t}) + C$.

The activation rate constant is subsequently calculated via the equation $k_{act} = k_{obs}/[I]_0$. $[I]_0$ is the initiator concentration at the beginning of the reaction which can be approximated to stay constant under pseudo-first-order conditions. Sample raw data and fit for all complexes are depicted in Figure S9-S14 in the SI. Values for k_{act} and k_{deact} are summarised in Table 4.

Table 4. k_{act} and k_{deact} for $[Cu(L)_2]Br$. L = GUAqu, GUA6etqu, GUA6buqu.

$[Cu(L)_2]Br$; L =	k_{act} [L mol^{-1} s^{-1}]	k_{deact} (= k_{act}/K_{ATRP}) [L mol^{-1} s^{-1}]
DMEGqu	$7.6\pm0.2\times10^{-1}$	$8.4\pm0.2\times10^{+6}$
TMGqu	$8.3\pm0.3\times10^{-1}$	$9.7\pm0.3\times10^{+6}$
DMEG6etqu	$1.2\pm0.1\times10^{0}$	$1.5\pm0.1\times10^{+7}$
TMG6etqu	$7.6\pm0.2\times10^{-1}$	$4.8\pm0.2\times10^{+6}$
DMEG6buqu	$8.3\pm0.9\times10^{-1}$	$1.1\pm0.9\times10^{+7}$
TMG6buqu	$9\pm1\times10^{-1}$	$7\pm1\times10^{+6}$

The values for k_{act} and k_{deact} for all six complexes are within the same order of magnitude. Only k_{act} of $[Cu(DMEG6etqu)_2]Br$, which exhibits a rather low value for K_{ATRP} seems to be extraordinarily high. The exceptional low solubility of $[Cu(DMEG6etqu)_2Br]Br$ in acetonitrile might influence the outcome of the k_{act} measurement.

All complexes exhibit sufficient values of K_{ATRP} and k_{deact} to find application in standard ATRP.[17]

Polymerisation kinetics:

Polymerisation kinetics with CuBr complexes of GUA6etqu and GUA6buqu were performed in bulk. We expected the complexes of alkyl substituted GUAqu ligands to be better soluble in styrene than the parent systems. It turned out, that the solubility of [Cu(DMEG6etqu)Br]Br in styrene is even worse in comparison to the complexes of the unsubstituted ligands. The poor solubility of the deactivator complex leads to termination of the ATRP reaction. Semilogarithmic kinetic plots and M_n and PD developments of ATRP reactions with $[Cu(DMEG6etqu)_2]Br$ and $[Cu(TMG6etqu)_2]Br$ are depicted in Figure S15 and S16 in the SI. On the contrary Cu^I and Cu^{II} complexes of GUA6buqu ligands are remarkably well soluble in pure styrene, even at room temperature. Figure 5 depicts semilogarithmic kinetic plots for styrene polymerisations mediated by $[Cu(DMEG6buqu)_2]Br$ and $[Cu(TMG6buqu)_2]Br$.

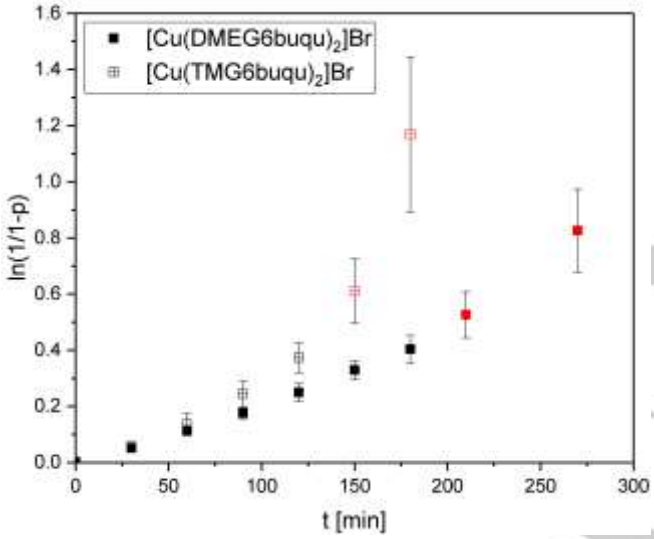

Figure 5. Semilogarithmic kinetic plots for styrene polymerisations in bulk mediated by $[Cu(DMEG6buqu)_2]Br$ and $[Cu(TMG6buqu)_2]Br$. Conditions: 110 °C; Ratio: monomer (styrene)/catalyst/ initiator (EBrib) = 100/1/1. Data points marked in red were not used for the calculation of k_{obs}.

At higher conversion, the viscosity of the reaction mixtures increases. Simultaneously acceleration of the polymerisation can be observed. This effect can be drawn back on auto-acceleration of the polymerisation reaction since the deactivation reaction becomes diffusion controlled in viscous media.[36]
Nevertheless, as can be seen in Figure 6, the ATRP proceeds very controlled, even at higher conversions of 60-70%.

Table 5. k_{obs} for $[Cu(DMEG6buqu)_2]Br$, $[Cu(TMG6buqu)_2]Br$, $[Cu(DMEGqu)_2]Br$ and $[Cu(TMGqu)_2]Br$. Styrene ATPR *in bulk*. Conditions: 110 °C for Br systems. Ratio: M/cat./init. = 100/1/1.

L=	DMEG6buqu	TMG6buqu	DMEGqu[6]	TMGqu[6]
$k_{obs}[s^{-1}]$	$3.4\pm0.2\times10^{-5}$	$4.7\pm0.3\times10^{-5}$	$5.4\pm0.1\times10^{-4}$	$2.3\pm0.1\times10^{-4}$

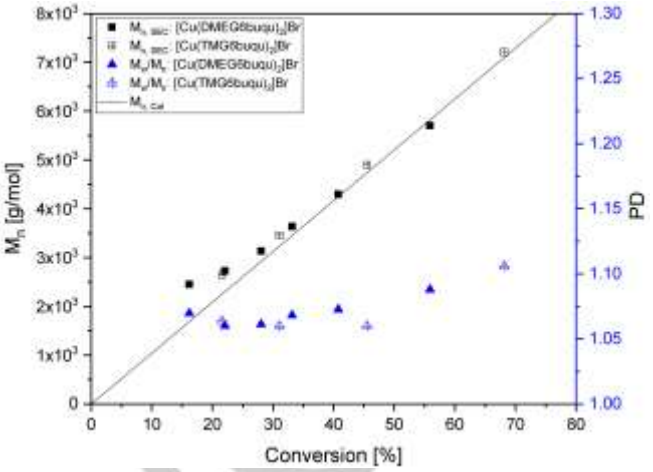

Figure 6. M_n and PD vs. conversion for styrene polymerisations in bulk mediated by $[Cu(DMEG6buqu)_2]Br$ and $[Cu(TMG6buqu)_2]Br$. Conditions: 110 °C; Ratio: monomer (styrene)/catalyst/initiator (EBrib) = 100/1/1.

Both systems reveal linear development of the molecular masses. The measured values for M_n are in accordance with expected theoretical ones. The values of PD are around 1.05 – 1.10 throughout the whole course of reaction but slightly increasing at higher conversion as the viscosity of the mixture rises. Table 5 summarises k_{obs} of the newly developed catalysts in comparison with k_{obs} of the parent complexes.[6] $[Cu(TMG6buqu)_2]Br$ reveals a higher k_{obs} in comparison to $[Cu(DMEG6buqu)_2]Br$. This is in accordance with the results of the K_{ATRP} determination, since $[Cu(TMG6buqu)_2]Br$ exhibits a higher value for K_{ATRP}. In comparison with the parent catalysts, complexes with DMEG6buqu and TMG6buqu show lower values for k_{obs}. Redox potentials and values of K_{ATRP} gave rise to the assumption, that k_{obs} of the new catalyst might be higher in comparison with the parent catalyst. But it has to be taken into account, that determinations of $E_{1/2}$ and K_{ATRP} are normally conducted in polar acetonitrile,[32] whereas polymerisations took place in apolar styrene. As shown by Matyjaszewski *et al.* K_{ATRP} is highly dependent on the nature of the solvent and K_{ATRP} values are usually smaller in apolar solvents.[32] The correlation of K_{ATRP} and k_{obs} might have been better, if the K_{ATRP} measurements were carried out in a more apolar solvent. Due to comparability with literature data, we restraint from performing K_{ATRP} measurements in a more apolar solvent. In comparison, the GUAbuqu systems allow a better controlled ATRP than their parent systems.

Prediction of Redox Properties and ATRP Activities

In a previous publication we showed, that with density functional theory, a suitable methodology and theoretical isodesmic reactions it is possible to predict the influence of even small differences in ligands on thermodynamic properties.[6] Here, we tested whether this concept could be used in future ligand design. In the case of the ethyl-substituted ligands, molecular structures of the Cu^I (activator) and Cu^{II} (deactivator) complexes could be obtained via X-ray crystallography. These served as starting geometries in DFT. In the case of butyl-substituted ligands no

crystallographic data was available. Starting geometries for GUA6buqu complexes were generated both from the molecular structures of GUAqu and GUA6etqu complexes.
Thus it should become possible to predict the thermodynamic properties of substituted GUAqu ligands without having their molecular structure at hands.

NBO Calculations

To receive closer insights into the effects of the substituent on the donor properties of the ligand, NBO calculations were performed with optimised structures of the ligands and the complexes. In the case of TMGqu, **L2** and **L4** no structural data was available, so starting geometries were generated from the structure of the corresponding DMEG ligands.
NBO charges give an indication of the influence of the substituent on the donor properties of the ligands.[37] Specific values are summarised Tables S5 and S6. NBO calculations on the ligands reveal, that an alkyl substitution at C6 increases the NBO charge at the N-donors. This effect is more pronounced in TMG ligands. Starting geometries for DMEG6etqu were generated both from the molecular structure of DMEGqu and DMEG6etqu. It is worth mentioning, that the NBO charges obtained by both methods differ significantly. This has to be kept in mind when thinking about *in silico* design of the new ligands.
Change from ethyl to butyl substitution does not alter the NBO charge at the donor atoms in case of TMG ligands. In DMEG ligands on the other hand the same substitution leads to a more positive NBO charge at N-donors, which seems counterintuitive.
Looking at the NBO charges within the Cu^{I} complexes, substituted DMEG and TMG ligands behave almost identically. The introduction of the alkyl substituent leads to a more negative charge at the metal centre, which underlines the improved donor properties of the ligands. The length of the alkyl substituent does not seem to have a significant influence.
In Cu^{II} bromido complexes similar trends are observable. With introduction of the alkyl substituent the NBO charge at the metal centre becomes more negative. In Cu^{II} chlorido complexes the alkyl substituents do not alter the NBO charge (DMEG) or even lead to a more positive NBO charge at the metal centre (TMG).
Generally it can be stated, that the introduction of an alkyl substituent at C6 of the quinoline leads to enhanced donor properties of the ligands. This is reflected in more negative NBO charges at the donor atoms if considering the bare ligands and (in most of the cases) more negative NBO charges at the metal centre in Cu^{I} and Cu^{II} complexes.

Isodesmic reactions: GUA6etqu vs. GUAqu

Geometry optimisation was followed by frequency calculation. Thermally corrected ΔG values were then inserted into the isodesmic equation (illustrated in Table 6). The isodesmic reaction provides ΔΔG, which gives relative information about the activity of the analysed complexes. Similar catalysts can be compared with regards to their thermodynamic properties. In case of GUAqu and GUA6etqu, starting geometries were directly generated from the molecular structures. Values for ΔΔG are summarised in Table 6. Comparing substituted and unsubstituted ligands 50 % of the isodesmic reactions are in accordance with experimental data. In the case of TMGqu vs. TMG6etqu, where a rather inactive catalyst is compared with one of the most active, the relative activity is predicted wrong. Comprehensive benchmarking on GUAqu copper complexes featuring non-coordinating counter-ions showed the influence of even small changes in the coordination angle on the relative energies.[38] If in our case the absolute minimum of the optimisation is not reached this might alter the outcome of the isodesmic reaction drastically and lead to a wrong prediction.

Table 6. ΔΔG values for theoretical isodesmic reactions with the ligands GUAqu and GUA6etqu. Basis set: def2-TZVP; Functional: TPSSh; Dispersion: GD3BJ.

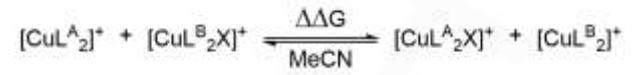

L^A vs. L^B / Transferred X	ΔΔG[kJ/mol]	Pred. correct?
DMEGqu vs. TMGqu / Br[6]	-4.8	Yes
DMEGqu vs. **L1** / Br	-10.0	Yes
DMEGqu vs. **L1** / Cl	-4.8	No
TMGqu vs. **L2** / Br	-3.1	No
TMGqu vs. **L2** / Cl	+4.3	Yes
L1 vs. **L2** / Br	+2.1	Yes
L1 vs. **L2** / Cl	-0.9	No

Isodesmic reactions: GUA6buqu vs. GUAqu

Starting geometries for GUA6buqu complexes were generated both from GUAqu and GUA6etqu complex structures. After geometry optimisation and frequency calculation, the obtained energies for the GUA6buqu complexes were compared to the energies of the unsubstituted parent systems via isodesmic reactions (illustrated in Table 7). In most of the cases the outcome of the isodesmic reaction does not agree with the experimental data or no sufficient statement can be made based on the present data. Furthermore, it seems to have no significant influence whether the starting geometries for the GUA6buqu complexes originated from the molecular structures of GUAqu or GUA6etqu. In Table 7 the difference between ΔΔG values obtained with starting geometries from GUAqu or GUA6etqu structures is also listed. It appeared, that the difference between both models lies within the same order of magnitude than the actual values of ΔΔG. A correct prediction of catalyst activities without structural data at hands thus seems not possible. With the longer butyl substituent even more structural conformers are possible in comparison with the ethyl-bearing ligands. Thus, it is even more complicated to find the absolute energy minimum.

Table 7. ΔΔG values for theoretical isodesmic reactions with the ligands GUAqu and GUA6buqu. Basis set: def2-TZVP; Functional: TPSSh; Dispersion: GD3BJ; SMD: MeCN.

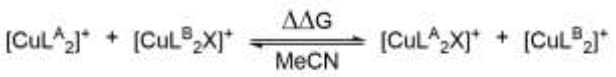

Origin:	GUAqu[a]		GUA6etqu[b]		
L^A vs. L^B / Transferred X	ΔΔG [kJ/mol]	Pred. corr.?	ΔΔG [kJ/mol]	Pred. corr.?	Diff.
DMEGqu vs. **L3** / Br	-0.1	?[c]	-6.4	Yes	6.3
DMEGqu vs. **L3** / Cl	-11.9	No	-4.4	No	7.5
TMGqu vs. **L4** / Br	~0	?[c]	-0.1	?[c]	~0
TMGqu vs. **L4** / Cl	1.2	Yes	-3.7	No	4.9
L3 vs. **L4** / Br	+4.8	No	+1.5	No	3.3
L3 vs. **L4** / Cl	-3.2	Yes	-9.2	Yes	6

[a]: Starting geometries for GUA6buqu complexes created from GUAqu complex structures.
[b]: Starting geometries for GUA6buqu complexes created from GUA6etqu complex structures.
[c]: No sufficient statement can be made based on the present data

As described above NBO calculations revealed high discrepancy between data generated from actual molecular structures and starting geometries that were designed *in silico*. Based on these results, it seems not possible to use isodesmic reactions in combination with *in silico* generated structures for the targeted design of new ATRP catalysts. Even when crystallographic data are available, the error rate is relatively high, especially when high conformational freedom is relevant. Moreover, it has to be remarked that the computed free energy differences lie close to the significance limit of DFT. Herein, we have explored the limit of the predictive power of the isodesmic equations.

Conclusion

The synthesis of four substituted guanidine quinoline (GUAqu) ligands was presented. The alkyl substituent in DMEG6etqu, TMG6etqu, DMEG6buqu and TMG6buqu should primarily lead to a better solubility of corresponding ATRP catalysts in apolar monomers. With the help of DFT and NBO calculations, the possible substitution positions were evaluated with respect to their electronic influence. With substitution at C6 of the quinoline backbone a compromise between electronic influence and synthetic accessibility was chosen. Our synthetic approach allows the synthesis of almost every 6-substituted GUAqu ligand starting from *para*-substituted anilines.

We discussed the structures of seven GUA6etqu copper complexes. Comparison of them reveals that the TMG moiety represents the stronger N-donor. In comparison with the parent ligands TMG6etqu shows better donor properties.

The redox potentials of copper complexes with GUA6alkqu complexes were determined via CV. The alkyl substituents at 6-position of the quinoline backbone yield reduced redox potentials in comparison with complexes of GUAqu in most cases. In copper bromido complexes featuring DMEG6etqu, the ethyl substituent has only a minor effect, whereas in TMG6etqu complexes the effect is more pronounced. This is also expressed in K_{ATRP} values. The alkyl substituent in DMEG-bearing ligands only has a minor activity of the corresponding complexes, whereas complexes of TMG6alkqu show the highest values for K_{ATRP} within the series. The values for k_{act} and k_{deact} for all six complexes are within the same order of magnitude. All complexes exhibit high values of K_{ATRP} and k_{deact} for application in standard ATRP.

Bulk ATRP experiments were conducted with the CuBr complexes of all ligands. As targeted, Cu^{I} and Cu^{II} complexes of GUA6buqu ligands are highly soluble in pure styrene. The catalysts revealed excellent control throughout the ATRP. In contrary to our expectations the deactivator species $[Cu(DMEG6etqu)_2Br]Br$ was only barely soluble in styrene. The butyl substituent in TMG6buqu leads to a lower redox potential, a higher K_{ATRP} value, better solubility in styrene and better polymerisation control.

With DFT, NBO and isodesmic reactions the influence of the substituent was further investigated. NBO showed that the alkyl substituents lead to improved donor properties of the ligands. But it also could be demonstrated that the result of the NBO calculation depends on the origin of the applied starting geometry. With isodesmic reactions and crystallographic data at hands (in case of GUA6etqu) correct activity predictions could be made in 50 % of the cases. The flexibility of the ethyl substituent leads to a higher conformational freedom and thus, the absolute minimum of a geometry optimisation might not be found. Starting geometries for GUA6buqu were generated both from complex structures of GUAqu and GUA6etqu. We evaluated whether new catalysts might be developed by simply generating them *in silico* from known structures and compare them with known catalysts via isodesmic reactions. It turned out, that the uncertainty of ΔΔG is within the same order of magnitude as the actual values of ΔΔG. Based on these results predictions of activities could not be made with sufficient accuracy.

To sum up, butylation of GUAqu leads to better solubility and enhanced ATRP activity of certain copper complexes. Our newly developed synthetic approach opens up an inexpensive way to modify GUAqu-ligands with respect to desired properties. We also showed up possibilities and limitations of our DFT method. Improvement of this method might open up ways for the development of tailor made ATRP catalysts

Experimental Section

General:

Ligand and complex syntheses were performed under inert conditions by using Schlenk techniques and a glove box under nitrogen atmosphere. Solvents were purified according to literature and kept under inert

conditions.[39] Chemicals for the synthesis of the ligands as well as Cu^{II}-salts for complex syntheses were all purchased from Grüssing, AppliChem, Acros Organics or TCI and were used as received without further purification. $Cu^{I}Br$, $Cu^{I}Cl$ and the Vilsmeier salts *N*,*N*'-dimethylethylenechloroformamidinium chloride (DMEG-VS) and *N*,*N*,*N*',*N*'-tetramethylchloroformamidinium chloride (TMG-VS) were synthesised as described in the literature.[28,40] The ligands DMEGqu and TMGqu were synthesised according to the literature.[41]

General analytical methods:

IR: KBr IR spectra were measured with a ThermoFisher Avatar 360 (Resolution 2 cm^{-1}). ATR IR spectra where measured with a Shimadzu IRTracer 100 with CsI beamsplitter in combination with a Specac Quest ATR unit (Resolution 2 cm^{-1}).

MS: EI mass spectra were obtained with a ThermoFisher Scientific Finnigan MAT 95 mass spectrometer. FAB mass spectra were obtained with a Thermo Finnigan MAT 95 or a Jeol MStation 700. Ionisation took place in 2-nitrobenzyl alcohol or glycerol as matrix on a copper target with 8 kV xenon atoms. ESI mass spectra were obtained with a ThermoFisher Scientific LTQ Orbitrap XL. The source voltage was 4.49 kV, the capillary temperature amounted to 299.54 °C. The tube lens voltage lay between 110 and 130 V.

^{1}H- and ^{13}C-NMR: ^{1}H- and ^{13}C-NMR spectra were measured on a Bruker Avance III HD 400 or a Bruker Avance II 400 nuclear resonance spectrometer. Measurements were performed in fully deuterated solvents. The residual signal of the solvent served as an internal standard.

Gel permeation chromatography:

The average molecular masses and the mass distributions of the obtained polystyrene samples were determined by gel permeation chromatography (GPC) in THF as mobile phase at a flow rate of 1 mL/min. The utilised GPCmax VE-2001 from Viscotek is a combination of an HPLC pump, two Malvern Viscotek T columns (porous styrene divinylbenzene copolymer) with a maximum pore size of 500 and 5000 Å and a refractive index detector (VE-3580) and a viscometer (Viscotek 270 Dual Detector). Universal calibration was applied to evaluate the chromatographic results.

UV/Vis setup for K_{ATRP}/k_{act} determination:

UV/Vis measurements were performed with an Avantes AvaSpec-ULS2048 CCD-Spectrometer and an Avantes AvaLight-DH-S-BAL lightsource. The measurements were done in Hellma QS-Screwcap-Cuvettes with an optical pathlength of 10.00 mm.

CV measurements:

The measurements were performed at room temperature under inert conditions with a Metrohm Autolab Potentiostat PGSTAT 101 using a three electrode arrangement with a Pt disc working electrode (1 mm diameter), a Pt wire as counter electrode and a Ag wire as reference electrode (pseudo reference). The measurements were performed in CH_3CN / 0.1 mol L^{-1} NBu_4PF_6 with a sample concentration of 10 mM. Ferrocene was added as an internal standard after the measurements of the sample and all potentials are referenced relative to the Fc/Fc^{+} couple. Cyclic voltammograms were measured with 200 mV/s, 100 mV/s, 50 mV/s and 20 mV/s.

X-ray diffraction analysis:

The single crystal diffraction data for **L1**, **L3** and **C1** to **C7** are presented in Tables S8-S10 . All data were collected on a Bruker D8 goniometer with APEX CCD detector. An Incoatec microsource with Mo-Kα radiation (λ = 0.71073 Å) was used and temperature control was achieved with an Oxford Cryostream 700. Crystals were mounted with grease on glass fibers and data were collected at 100 K in ω-scan mode. Data were collected with SMART[42], integrated with SAINT[42] and corrected for absorption by multi-scan methods with SADABS.[41] The structure was solved by direct and conventional Fourier methods and all non-hydrogen atoms were refined anisotropically with full-matrix least-squares based on F^2 (XPREP[43], SHELXS-97[44] and ShelXle[45]). Hydrogen atoms were derived from difference Fourier maps and placed at idealised positions, riding on their parent C atoms, with isotropic displacement parameters $U_{iso}(H) = 1.2U_{eq}(C)$ and $1.5U_{eq}$(C methyl). All methyl groups were allowed to rotate but not to tip.

In **C2** it was not possible to model the disordered solvent molecules (THF) in an adequate manner, and the data set was treated with the SQUEEZE routine as implemented in PLATON.[46,47]

In **C6**, the space group was checked with the ADDSYM routine as implemented in Platon[46,47] and ADDSYM suggested pseudo-translations (A-face centered) or the space group C2/c. Also a B-alert of the checkcif-routine occured. The data of this complex show no integral reflections, and the most disagreeable reflections are also unobstrusive. Furthermore, in $P2_1/n$ only 2229 reflections from 87813 were rejected and in the centered space-groups 50% of the reflections were rejected, e.g. in *C*2/c 45041 from 87813. Also the structure solution in the centered space-groups are not suited. Hence, a pseudo-symmetry is present.

Full crystallographic data (excluding structure factors) have been deposited with the Cambridge Crystallographic Data Centre as supplementary no. CCDC – 1820775 for **L1**, CCDC – 1820776 for **L3**, CCDC – 1820777 for **C1**, CCDC – 1820778 for **C2**, CCDC – 1820779 for **C3**, CCDC – 1820780 for **C4**, CCDC – 1820781 for **C5**, CCDC – 1820782 for **C6** and CCDC – 1820783 for **C7**. Copies of the data can be obtained free of charge on application to CCDC, 12 Union Road, Cambridge CB2 1EZ, UK (fax: (+44)1223-336-033; e-mail: deposit@ccdc.cam.ac.uk).

Computational details

Density functional theory (DFT) calculations were carried out with Gaussian09 Revision D.01.[48] All calculations were performed using the TPSSh [21] functional and def2-TZVP basis sets.[20] Starting geometries for optimisation were generated from the crystal structures of DMEGqu, DMEG6etqu, DMEG6buqu, $[Cu(DMEGqu)_2]Br$, $[Cu(TMGqu)_2]Br$, $[Cu(DMEGqu)_2]Cl$, $[Cu(TMGqu)_2]Cl$, $[Cu(DMEGqu)_2Br]Br$, $[Cu(TMGqu)_2Br]Br$, $[Cu(DMEGqu)_2Cl]Cl$, $[Cu(TMGqu)_2Cl]Cl$ $[Cu(DMEG6etqu)_2]Br$, $[Cu(TMG6etqu)_2]Br$, $[Cu(DMEG6etqu)_2]Cl$, $[Cu(TMG6etqu)_2]Cl$, $[Cu(DMEG6etqu)_2Br]Br$, $[Cu(TMG6etqu)_2Br]Br$, $[Cu(DMEG6etqu)_2Cl]Cl$ and $[Cu(TMG6etqu)_2Cl]Cl$. To receive thermal corrected values of ΔG, frequency calculations at room temperature (25 °C) were performed. Calculations were conducted both in gas phase and in solvent using the SMD model[25] with the implemented solvent acetonitrile. All calculations were performed with Grimme dispersion and Becke-Johnson damping GD3BJ.[22,23,49] NBO calculations were performed with the NBO 6.0 software.[50]

Polymerisation procedure:

Styrene (Acros Organics, 99 % stab.) and the initiator ethyl α-bromoisobutyrate (EBrib, abcr, 98 %) have been freshly distilled over CaH_2. All polymerisations were performed with *in situ* generated catalysts. First the copper salt (0.19 mmol, $Cu^{I}Br$: 27 mg) then ligand (0.38 mmol, DMEG6etqu: 102 mg, TMG6etqu: 103 mg, DMEG6buqu: 113 mg, TMG6buqu: 113 mg) were directly weighed into the polymerisation vessel under inert conditions inside a glovebox. Outside the glove box the prepared Schlenk tube was then connected to a Schlenk line. Styrene

(19 mmol, 2.2 mL) and finally the initiator (0.19 mmol, EBrib: 28 µL) were added with gastight glass syringes.

After addition of the initiator, the mixture was heated (110 °C) under vigorous stirring. The first sample was taken with a glass pipette under inert conditions after 2.5 min. At this point of time the polymerisation mixture reached its desired temperature and thus was chosen to be starting point of the polymerisation. Further samples were taken in certain time intervals. The samples were mixed with $CDCl_3$ and the conversion measured by ^{1}H-NMR spectroscopy. Afterwards the polymer was precipitated in ethanol to remove the copper compound and residual monomer. The solid, colourless polystyrene was dried overnight and molecular mass distributions were determined by GPC.

K_{ATRP} determination:

All measurements were performed in oxygen free acetonitrile at 22 °C. The acetonitrile has been degassed by three *freeze-pump-thaw* cycles. Stock solutions of the complexes and the cuvettes were prepared in a glovebox under inert conditions.

First, stock solutions of the initiator (147 µL (1.00 mmol) EBrib in 10 mL of acetonitrile) and the complexes (0.05 mmol $Cu^{I}Br$ (7.2 mg) and 0.1 mmol ligand (DMEGqu: 24.0 mg; TMGqu: 24.2 mg; DMEG6etqu: 26.8 mg; TMG6etqu: 27.0 mg; DMEG6buqu: 29.6 mg; TMG6buqu: 29.8 mg) in 2 mL of acetonitrile) were prepared. A screw cap cuvette containing a stirring bar was filled with 1.5 mL of acetonitrile and tightly sealed with a silicon septum. After addition of 400 µL catalyst solution the UV/Vis measurement was started. By adding 100 µL of EBrib solution the reaction was initiated and the formation of the Cu^{II} species was followed via UV/Vis spectroscopy.

k_{act} determination:

All measurements were performed in oxygen free acetonitrile at 22 °C. The acetonitrile has been degassed by three *freeze-pump-thaw* cycles. Stock solutions of the complexes and the cuvettes were prepared in a glovebox under inert conditions. First, stock solutions of the initiator (880 µL (6.00 mmol) EBrib in 10 mL of solvent), the trapping agent (234 mg TEMPO in 10 mL solvent) and the complexes (0.05 mmol $Cu^{I}Br$ and 0.1 mmol ligand in 2 mL of solvent) were prepared.

A screw cap cuvette containing a stirring bar was filled with 1.26 mL acetonitrile and tightly sealed with a silicon septum. After addition of 100 µL initiator and 400 µL TEMPO solution the UV/Vis measurement was started. By adding 240 µL of complex solution the reaction was initiated and the formation of the Cu^{II} species was followed via UV/Vis spectroscopy.

Acknowledgements

Financial support by the Fonds der Chemischen Industrie (Fonds fellowships for T.R.) is gratefully acknowledged. Moreover, we thank for granted calculation time from the OCuLUS Cluster at the PC^2 Paderborn and the Cheops Cluster at the RRZK Cologne.

Keywords: Copper • ATRP • Guanidine • Molecular structure • Density functional theory

[1] a) M. Kato, T. Ando, M. Sawamoto, M. Kato, M. Kamigaito, M. Sawamoto, T. Higashimura, *Macromolecules* **1995**, *28*(5), 1721–1723; b) J.-S. Wang, K. Matyjaszewski, *Macromolecules* **1995**, *28*(23), 7901–7910; c) V. Percec, B. Barboiu, *Macromolecules* **1995**, *28*(23), 7970–7972; d) K. Matyjaszewski, *Macromolecules* **2012**, *45*(10), 4015–4039;

[2] a) K. Min, H. Gao, K. Matyjaszewski, *J. Am. Chem. Soc.* **2005**, *127*(11), 3825–3830; b) W. Jakubowski, K. Matyjaszewski, *Angew. Chem. Int. Ed.* **2006**, *45*(27), 4482–4486, *Angew. Chem.* **2006**, *118*(27), 4594–4598; c) A. J. D. Magenau, N. C. Strandwitz, A. Gennaro, K. Matyjaszewski, *Science* **2011**, *332*(6025), 81–84; d) N. Bortolamei, A. A. Isse, A. J. D. Magenau, A. Gennaro, K. Matyjaszewski, *Angew. Chem. Int. Ed.* **2011**, *50*(48), 11391–11394, *Angew. Chem.* **2011**, *123*(48), 11593–11596;

[3] W. Tang, K. Matyjaszewski, *Macromolecules* **2006**, *39*(15), 4953–4959.

[4] A. J. D. Magenau, Y. Kwak, K. Schröder, K. Matyjaszewski, *ACS Macro Lett.* **2012**, *1*(4), 508–512.

[5] T. G. Ribelli, M. Fantin, J.-C. Daran, K. F. Augustine, R. Poli, K. Matyjaszewski, *J. Am. Chem. Soc.* **2018**, DOI: 10.1021/jacs.7b12180.

[6] T. Rösener, O. Bienemann, K. Sigl, N. Schopp, F. Schnitter, U. Flörke, A. Hoffmann, A. Döring, D. Kuckling, S. Herres-Pawlis, *Chem. Eur. J.* **2016**, *22*(38), 13550–13562.

[7] A. Hoffmann, O. Bienemann, I. dos Santos Vieira, S. Herres-Pawlis, *Polymers* **2014**, *6*(4), 995–1007.

[8] A. Hoffmann, O. Bienemann, I. dos Santos Vieira, S. Herres-Pawlis, *Z. Naturf. B* **2014**, *69*(5), 589–595.

[9] O. Bienemann, A.-K. Froin, I. dos Santos Vieira, R. Wortmann, A. Hoffmann, S. Herres-Pawlis, *Z. anorg. allg. Chem.* **2012**, *638*(11), 1683–1690.

[10] O. Bienemann, R. Haase, A. Jesser, T. Beschnitt, A. Döring, D. Kuckling, I. dos Santos Vieira, U. Flörke, S. Herres-Pawlis, *Eur. J. Inorg. Chem.* **2011**, *2011*(15), 2367–2379.

[11] O. Bienemann, R. Haase, U. Flörke, A. Döring, D. Kuckling, S. Herres-Pawlis, *Z. Naturf.* **2010**, *65b*, 798–806.

[12] a) A. Metz, R. Plothe, B. Glowacki, A. Koszalkowski, M. Scheckenbach, A. Beringer, T. Rösener, J. Michaelis de Vasconcellos, R. Haase, U. Flörke, A. Hoffmann, S. Herres-Pawlis, *Eur. J. Inorg. Chem.* **2016**, *2016*(31), 4974–4987; b) P. M. Schäfer, M. Fuchs, A. Ohligschläger, R. Rittinghaus, P. McKeown, E. Akin, M. Schmidt, A. Hoffmann, M. A. Liauw, M. D. Jones, S. Herres-Pawlis, *ChemSusChem* **2017**, *10*(18), 3547–3556; c) N. G. Sedush, V. V. Izraylit, A. K. Mailyan, D. V. Savinov, Y. I. Kiryukhin, S. N. Chvalun, *Mendeleev Commun.* **2017**, *27*(3), 281–282;

[13] a) F. Strassl, B. Grimm-Lebsanft, D. Rukser, F. Biebl, M. Biednov, C. Brett, R. Timmermann, F. Metz, A. Hoffmann, M. Rübhausen, S. Herres-Pawlis, *Eur. J. Inorg. Chem.* **2017**, *2017*(27), 3350–3359; b) S. Herres-Pawlis, R. Haase, P. Verma, A. Hoffmann, P. Kang, T. D. P. Stack, *Eur. J. Inorg. Chem.* **2015**, *2015*(32), 5426–5436;

[14] a) S. H. Oakley, M. P. Coles, P. B. Hitchcock, *Inorg. Chem.* **2003**, *42*(10), 3154–3156; b) A. S. Brar, S. Kaur, *J. Polym. Sci. A Polym. Chem.* **2005**, *43*(23), 5906–5922;

[15] B. Dicke, A. Hoffmann, J. Stanek, M. S. Rampp, B. Grimm-Lebsanft, F. Biebl, D. Rukser, B. Maerz, D. Göries, M. Naumova, M. Biednov, G. Neuber, A. Wetzel, S. M. Hofmann, P. Roedig, A. Meents, J. Bielecki, J. Andreasson, K. R. Beyerlein, H. N. Chapman, C. Bressler, W. Zinth, M. Rübhausen, S. Herres-Pawlis, *Nature Chem* **2018**, *59*, DOI: 10.1038/nchem.2916.

[16] a) J. Stanek, N. Sackers, F. Fink, M. Paul, L. Peters, R. Grunzke, A. Hoffmann, S. Herres-Pawlis, *Chem. Eur. J.* **2017**, *23*(62), 15738–15745; b) A. Hoffmann, J. Stanek, B. Dicke, L. Peters, B. Grimm-Lebsanft, A. Wetzel, A. Jesser, M. Bauer, M. Gnida, W. Meyer-Klaucke, M. Rübhausen, S. Herres-Pawlis, *Eur. J. Inorg. Chem.* **2016**, *2016*(29), 4731–4743;

[17] W. Tang, Y. Kwak, W. Braunecker, N. V. Tsarevsky, M. L. Coote, K. Matyjaszewski, *J. Am. Chem. Soc.* **2008**, *130*, 10702–10713.

[18] a) T. F. Hughes, R. A. Friesner, *J. Chem. Theory Comput.* **2012**, *8*(2), 442–459; b) S. J. Konezny, M. D. Doherty, O. R. Luca, R. H. Crabtree, G. L. Soloveichik, V. S. Batista, *J. Phys. Chem. C* **2012**, *116*(10), 6349–6356;

[19] C. J. Cramer, *Essentials of computational chemistry*: Theories and models; Wiley, Chichester, **2004**.

[20] F. Weigend, R. Ahlrichs, *Phys. Chem. Chem. Phys.* **2005**, *7*(18), 3297–3305.

[21] V. N. Staroverov, G. E. Scuseria, J. Tao, J. P. Perdew, *J. Chem. Phys.* **2009**, 12129–12137.

[22] L. Goerigk, S. Grimme, *Phys. Chem. Chem. Phys.* **2011**, *13*(14), 6670–6688.

[23] S. Grimme, S. Ehrlich, L. Goerigk, *J. Comp. Chem.* **2011**, 1456–1465.

[24] A. Hoffmann, R. Grunzke, S. Herres-Pawlis, *J. Comput. Chem.* **2014**, *35*(27), 1943–1950.

[25] A. V. Marenich, C. J. Cramer, D. G. Truhlar, *J. Phys. Chem. B* **2009**, *113*(18), 6378–6396.

[26] K. R. Buszek, N. Brown, D. Luo, *Org. lett.* **2009**, *11*(1), 201–204.

[27] G. Wielgosz-Collin, M. Duflos, P. Pinson, G. Le Baut, P. Renard, C. Bennejean, J. Boutin, M. Boulanger, *J. Enzym. Inhib. Med. Chem.* **2002**, *17*(6), 449–453.

[28] W. Kantlehner, E. Haug, W. W. Mergen, P. Speh, T. Maier, J. J. Kapassakalidis, H.-J. Bräuner, H. Hagen, *Liebigs Ann. Chem.* **1984**, *1984*(1), 108–126.

[29] S. Herres-Pawlis, U. Flörke, G. Henkel, *Eur. J. Inorg. Chem.* **2005**, *2005*(19), 3815–3824.

[30] A. Hoffmann, S. Binder, A. Jesser, R. Haase, U. Flörke, M. Gnida, M. Salomone Stagni, W. Meyer-Klaucke, B. Lebsanft, L. E. Grünig, S. Schneider, M. Hashemi, A. Goos, A. Wetzel, M. Rübhausen, S. Herres-Pawlis, *Angew. Chem. Int. Ed.* **2014**, *53*(1), 299–304, *Angew. Chem.* **2014**, *126*(1), 305–310.
[31] N. G. Connelly, W. E. Geiger, *Chem. Rev.* **1996**, *96*(2), 877–910.
[32] W. A. Braunecker, N. V. Tsarevsky, A. Gennaro, K. Matyjaszewski, *Macromolecules* **2009**, *42*(17), 6348–6360.
[33] W. Tang, N. V. Tsarevsky, K. Matyjaszewski, *J. Am. Chem. Soc.* **2006**, *128*(5), 1598–1604.
[34] a) K. Matyjaszewski, H. Paik, P. Zhou, S. J. Diamanti, *Macromolecules* **2001**, *34*(15), 5125–5131; b) J. Gromada, K. Matyjaszewski, *Macromolecules* **2002**, *35*(16), 6167–6173;
[35] M. Horn, K. Matyjaszewski, *Macromolecules* **2013**, *46*(9), 3350–3357.
[36] a) A. R. Wang, S. Zhu, *Macromolecules* **2002**, *35*(27), 9926–9933; b) A. Rabea, S. Zhu, *Polymers* **2015**, *7*(5), 819–835.
[37] a) A. Hoffmann, S. Herres-Pawlis, *Phys. Chem. Chem. Phys.* **2016**, *18*(9), 6430–6440; b) P. Liebhäuser, K. Keisers, A. Hoffmann, T. Schnappinger, I. Sommer, A. Thoma, C. Wilfer, R. Schoch, K. Stührenberg, M. Bauer, M. Dürr, I. Ivanović-Burmazović, S. Herres-Pawlis, *Chem. Eur. J.* **2017**, *23*(50) 12171-12183;
[38] A. Jesser, M. Rohrmüller, W. G. Schmidt, S. Herres-Pawlis, *J. Comput. Chem.* **2014**, *35*(1), 1–17.
[39] A. J. Niestroj, M. E. Maier, *Praxis in der Organischen Chemie;* VCH, Weinheim, **1997**.
[40] H.-D. Hardt, *Z. anorg. allg. Chem.* **1959**, *301*(1-2), 87–96.
[41] A. Hoffmann, J. Börner, U. Flörke, S. Herres-Pawlis, *Inorg. Chim. Acta* **2009**, *362*(4), 1185–1193.
[42] Bruker, *SMART (Version 5.62), SAINT (Version 8.18C, 2011), SHELXTL (Version 6.10), SADABS (Version V2012/1);* AXS Inc, Madison, Wisconsin, USA, **2002**.
[43] Bruker, *XPREP;* AXS Inc, Madison, Wisconsin, USA, **2007**.
[44] G. M. Sheldrick, *Acta Cryst, Sect. A* **1990**, *46*(6), 467–473.
[45] C. B. Hübschle, G. M. Sheldrick, B. Dittrich, *J. Appl. Crystallogr.* **2011**, *44*(6), 1281–1284.
[46] A. L. Spek, *PLATON, A Multipurpose Crystallographic Tool*, Utrecht University, Utrecht (The Netherlands), **2008**.
[47] A. L. Spek, *Acta Cryst, Sect. D* **2009**, *65*, 148–155.
[48] M. J. Frisch, G. W. Trucks, H. B. Schlegel, G. E. Scuseria, M. A. Robb, J. R. Cheeseman, G. Scalmani, V. Barone, B. Mennucci, G. A. Petersson, H. Nakatsuji, M. Caricato, X. Li, H. P. Hratchian, A. F. Izmaylov, J. Bloino, G. Zheng, J. L. Sonnenberg, M. Hada, M. Ehara, K. Toyota, R. Fukuda, J. Hasegawa, M. Ishida, T. Nakajima, Y. Honda, O. Kitao, H. Nakai, T. Vreven, J. A. Montgomery, JR, J. E. Peralta, F. Ogliaro, M. Bearpark, J. J. Heyd, E. Brothers, K. N. Kudin, V. N. Staroverov, R. Kobayashi, J. Normand, K. Raghavachari, A. Rendell, J. C. Burant, S. S. Iyengar, J. Tomasi, M. Cossi, N. Rega, J. M. Millam, M. Klene, J. E. Knox, J. B. Cross, V. Bakken, C. Adamo, J. Jaramillo, R. Gomperts, R. E. Stratmann, O. Yazyev, A. J. Austin, R. Cammi, C. Pomelli, J. W. Ochterski, R. L. Martin, K. Morokuma, V. G. Zakrzewski, G. A. Voth, P. Salvador, J. J. Dannenberg, S. Dapprich, A. D. Daniels, O. Farkas, J. B. Foresman, J. V. Ortiz, J. Cioslowski, D. J. Fox, *Gaussian 09, Revision D.01;* Gaussian, Inc, Wallingford CT, **2013**.
[49] A. Hoffmann, R. Grunzke, S. Herres-Pawlis, *J. Comput. Chem.* **2014**, *35*(27), 1943–1950.
[50] E. D. Glendening, J. K. Badenhoop, A. E. Reed, J. E. Carpenter, J. A. Bohmann, C. M. Morales, C. R. Landis, F. Weinhold, *NBO 6.0.;* Theoretical Chemistry Institute, University of Wisconsin, Madison, Wisconsin, USA, **2013**.

10.1002/ejic.201800511

WILEY-VCH

Entry for the Table of Contents (Please choose one layout)

Layout 1:

FULL PAPER

A synthetic approach towards C6 substituted guanidine quinoline ligands is presented. $Cu^{I}X$ and $Cu^{II}X_2$ (X = Br or Cl) complexes of alkylated ligands DMEG6etqu, TMG-6etqu, DMEG6buqu and TMG6buqu are investigated with regard to their structures, redox potential and activity in ATRP. By DFT, NBO and isodesmic reactions the influence of substituents on the electrochemistry and ATRP properties was further examined.

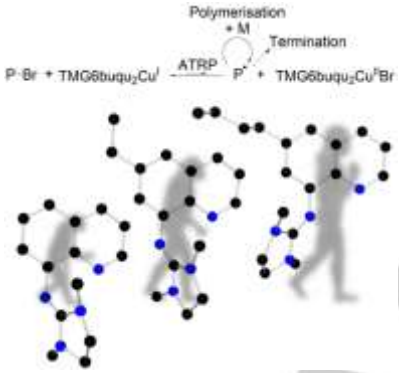

Thomas Rösener, Alexander Hoffmann and Sonja Herres-Pawlis

Page No. – Page No.

Next Generation of Guanidine Quinoline Copper Complexes for Highly Controlled ATRP: Influence of Backbone Substitution on Redox Chemistry and Solubility